Control of integrated micro-resonator wavelength via balanced homodyne locking

Jonathan A. Cox,[*] Anthony L. Lentine, Douglas C. Trotter, and Andrew L. Starbuck

Sandia National Laboratories, P.O. Box 5800, Albuquerque, NM, 87185 USA
[*]*joncox@alum.mit.edu*

Abstract: We describe and experimentally demonstrate a method for active control of resonant modulators and filters in an integrated photonics platform. Variations in resonance frequency due to manufacturing processes and thermal fluctuations are corrected by way of balanced homodyne locking. The method is compact, insensitive to intensity fluctuations, minimally disturbs the micro-resonator, and does not require an arbitrary reference to lock. We demonstrate long-term stable locking of an integrated filter to a laser swept over 1.25 THz. In addition, we show locking of a modulator with low bit error rate while the chip temperature is varied from 5 to 60° C.

OCIS codes: (200.4650) Optical interconnects; (130.0130) Integrated optics; (120.3180) Interferometry; (130.7408) Wavelength filtering devices; (130.4110) Modulators; (130.6750) Systems.

References and links

1. M. R. Watts, W. A. Zortman, D. C. Trotter, R. W. Young, and A. L. Lentine, "Vertical junction silicon microdisk modulators and switches," Opt. Express **19**(22), 21989–22003 (2011).
2. W. Zortman, A. Lentine, D. Trotter, and M. Watts, "Integrated CMOS comaptible low power 10Gbps silicon photonic heater modulator," in *Optical Fiber Communication Conference*, OSA Technical Digest (Optical Society of America, 2012), paper OW4I.5.
3. M. Lipson, "Compact electro-optic modulators on a silicon chip," IEEE J. Sel. Top. Quantum Electron. **12**(6), 1520–1526 (2006).
4. J. S. Levy, A. Gondarenko, M. A. Foster, A. C. Turner-Foster, A. L. Gaeta, and M. Lipson, "CMOS-compatible multiple-wavelength oscillator for on-chip optical interconnects," Nat. Photonics **4**(1), 37–40 (2010).
5. A. Schliesser, P. Del'Haye, N. Nooshi, K. J. Vahala, and T. J. Kippenberg, "Radiation pressure cooling of a micromechanical oscillator using dynamical backaction," Phys. Rev. Lett. **97**(24), 243905 (2006).
6. G. Cocorullo, F. G. Della Corte, and I. Rendina, "Temperature dependence of the thermo-optic coefficient in crystalline silicon between room temperature and 550 K at the wavelength of 1523 nm," Appl. Phys. Lett. **74**(22), 3338 (1999).
7. V. R. Almeida and M. Lipson, "Optical bistability on a silicon chip," Opt. Lett. **29**(20), 2387–2389 (2004).
8. W. A. Zortman, D. C. Trotter, and M. R. Watts, "Silicon photonics manufacturing," Opt. Express **18**(23), 23598–23607 (2010).
9. A. V. Krishnamoorthy, Xuezhe Zheng, Guoliang Li, Jin Yao, T. Pinguet, A. Mekis, H. Thacker, I. Shubin, Ying Luo, K. Raj, and J. E. Cunningham, "Exploiting CMOS manufacturing to reduce tuning requirements for resonant optical devices," IEEE Photonics J. **3**(3), 567–579 (2011).
10. V. Raghunathan, W. N. Ye, J. Hu, T. Izuhara, J. Michel, and L. Kimerling, "Athermal operation of Silicon waveguides: spectral, second order and footprint dependencies," Opt. Express **18**(17), 17631–17639 (2010).
11. H. L. R. Lira, S. Manipatruni, and M. Lipson, "Broadband hitless silicon electro-optic switch for on-chip optical networks," Opt. Express **17**(25), 22271–22280 (2009).
12. J. E. Cunningham, I. Shubin, X. Zheng, T. Pinguet, A. Mekis, Y. Luo, H. Thacker, G. Li, J. Yao, K. Raj, and A. V. Krishnamoorthy, "Highly-efficient thermally-tuned resonant optical filters," Opt. Express **18**(18), 19055–19063 (2010).
13. G. Li, X. Zheng, J. Yao, H. Thacker, I. Shubin, Y. Luo, K. Raj, J. E. Cunningham, and A. V. Krishnamoorthy, "25Gb/s 1V-driving CMOS ring modulator with integrated thermal tuning," Opt. Express **19**(21), 20435–20443 (2011).
14. M. R. Watts, "Adiabatic microring resonators," Opt. Lett. **35**(19), 3231–3233 (2010).
15. K. Padmaraju, J. Chan, L. Chen, M. Lipson, and K. Bergman, "Thermal stabilization of a microring modulator using feedback control," Opt. Express **20**(27), 27999–28008 (2012).
16. E. Timurdogan, A. Biberman, D. C. Trotter, C. Sun, M. Moresco, V. Stojanovic, and M. R. Watts, "Automated wavelength recovery for microring resonators," in *Conference on Lasers and Electro-Optics 2012*, OSA Technical Digest (Optical Society of America, 2012), paper CM2M.1.

17. C. T. DeRose, M. R. Watts, D. C. Trotter, D. L. Luck, G. N. Nielson, and R. W. Young, "Silicon microring modulator with integrated heater and temperature sensor for thermal control," in *Conference on Lasers and Electro-Optics 2010*, OSA Technical Digest (Optical Society of America, 2010), paper CThJ3.
18. W. Zortman, A. Lentine, D. Trotter, and M. Watts, "Bit-error-rate monitoring for active wavelength control of resonant modulators," IEEE Micro **33**, 42–52 (2012).
19. K. Padmaraju, D. F. Logan, T. Shiraishi, J. J. Ackert, A. P. Knights, and K. Bergman, "Wavelength locking and thermally stabilizing microring resonators using dithering signals," J. Lightwave Technol. **32**(3), 505–512 (2014).
20. J. Chambers, "High frequency Pound-Drever-Hall optical ring resonator sensing," Master's thesis, Texas A&M University (2007).
21. C. Qiu, J. Shu, Z. Li, X. Zhang, and Q. Xu, "Wavelength tracking with thermally controlled silicon resonators," Opt. Express **19**(6), 5143–5148 (2011).
22. J. A. Cox, D. C. Trotter, and A. L. Starbuck, "Integrated control of silicon-photonic micro-resonator wavelength via balanced homodyne locking," in *Optical Interconnects Conference 2013* (IEEE, 2013), pp. 52–53.
23. M. Heurs, I. R. Petersen, M. R. James, and E. H. Huntington, "Homodyne locking of a squeezer," Opt. Lett. **34**(16), 2465–2467 (2009).
24. C. T. DeRose, D. C. Trotter, W. A. Zortman, A. L. Starbuck, M. Fisher, M. R. Watts, and P. S. Davids, "Ultra compact 45 GHz CMOS compatible Germanium waveguide photodiode with low dark current," Opt. Express **19**(25), 24897–24904 (2011).
25. M. R. Watts, J. Sun, C. DeRose, D. C. Trotter, R. W. Young, and G. N. Nielson, "Adiabatic thermo-optic Mach-Zehnder switch," Opt. Lett. **38**(5), 733–735 (2013).
26. W. A. Zortman, A. L. Lentine, D. C. Trotter, and M. R. Watts, "Low-voltage differentially-signaled modulators," Opt. Express **19**(27), 26017–26026 (2011).

1. Introduction

Integrated optical micro-resonators have been investigated for a wide range of applications, including micro-ring modulators [1–3] and filters, Kerr frequency comb generation [4] and even nano-opto-mechanical systems (NOMS) [5]. Micro-resonators are promising for next-generation dense wavelength division multiplexing (DWDM) communications systems for supercomputing and data centers, owing to their exceptionally low energy per bit and compact size. However, aligning the pump or signal beam wavelength with the micro-resonator wavelength is severely challenged by the thermo-optic sensitivity of the resonator, especially for silicon—which has a high thermo-optic coefficient [6]. In fact, the self-heating of the optical beam can significantly tune the resonant wavelength of the resonator in a bistable manner [7]. In addition, it is typically very difficult, if not impossible, to precisely fabricate a silicon micro-resonator to a given wavelength channel [8,9].

One approach for overcoming the thermal sensitivity is material athermalization, typically achieved with the use of a polymer of opposite thermal coefficient [10]. While early results are encouraging, an additional material must be incorporated into the CMOS process and the filters would still need to be individually tuned after fabrication. Moreover, athermalization has not been demonstrated for gigabit-class silicon modulators. Regardless, for many applications, such as Reconfigurable Optical Add Drop Multiplexers (ROADM), wavelength tuning is inherently necessary [11]. In any event, micro-resonators for NOMS or Kerr comb generation are highly constrained by the required phononic or dispersive properties, rendering athermalization difficult to achieve.

Efficient active control of micro-resonator wavelength is a critical for the wide-scale deployment of micro-resonators. Integrated micro-heaters have been proposed for silicon photonic modulators and filters as a method for shifting the device resonant wavelength to that of the incident laser [2,12–14]. To date, several techniques for locking modulators and filters have been demonstrated, including power transmission [15,16], temperature sensing [17], bit error rate monitoring [18], dither locking [19], Pound-Drever-Hall [20] and scattered optical power [21]. However, each scheme has certain drawbacks. Power monitoring requires an arbitrary reference that must be periodically recalibrated as the link intensity drifts. On the other hand, dither locking does not require a reference and can uniquely determine tuning direction, but necessitates more complex electronics to recover the error signal, such as a lock-in amplifier. Dither locking also disturbs the resonator in a way that can degrade the performance for very precise locking applications. Temperature sensing has not been capable of the high precision necessary for high-Q silicon resonators, and requires tradeoffs in the

device design [17]. Bit error rate monitoring is quite suitable for modulator stabilization, but cannot be used for filters and requires high speed logic which tends to consume significant power. Scattered optical power is not a scalable approach with the present implementation. Finally, the Pound-Drever-Hall method has not been integrated on chip yet, and requires disturbing the optical signal with a high speed phase modulator, as well as additional electronics to demodulate the error signal.

As a result, we developed a wavelength control scheme based on balanced homodyne detection that is suitable for filters and modulators, is insensitive to intensity fluctuations, does not disturb the optical signal or resonator and requires only the simplest control electronics, which are readily fabricated in modern CMOS nodes [22].

2. Balanced homodyne detection locking

Balanced homodyne detection of light coupled into a resonator is a general purpose technique for precisely interrogating the intrinsic phase and amplitude properties of a resonant cavity without disturbing either the signal beam or the resonator. In this way, it is a powerful technique for actively locking micro-resonators to a signal beam.
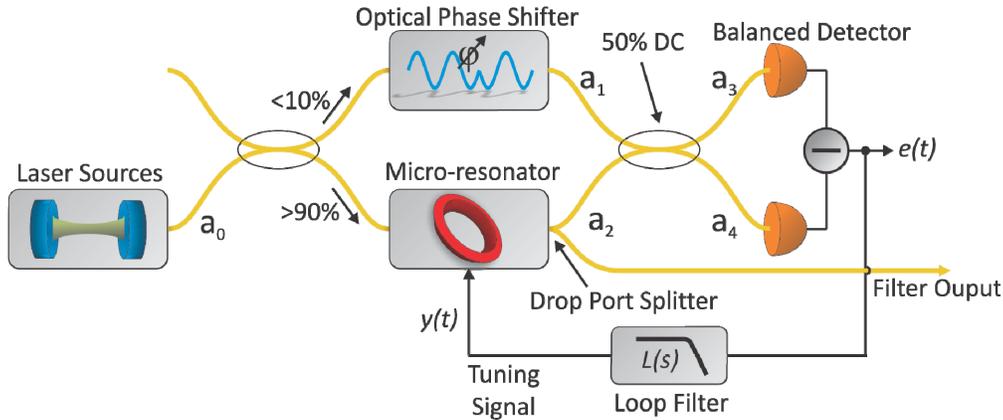

Fig. 1. Signal diagram of the balanced homodyne locking (BHL) method. A Mach-Zehnder interferometer (MZI) is formed by splitting the waveguide input between the micro-resonator and a phase shifter, before recombining on a balanced photodetector with a 50% directional coupler (**DC**). The resulting error signal, _e(t)_, drives the loop filter to tune the resonator. The locking point is adjusted by varying the phase shift.

Balanced homodyne locking (BHL) can be understood as the balanced detection of an unbalanced, four port Mach-Zehnder Interferometer (MZI) where the micro-resonator (or other optical element) is inserted in one path. An optical phase shifter may optionally be inserted in the other, as in Fig. 1, in order to adjust the locking point. First, a small percentage of power, from the input port to the micro-resonator is tapped off by the left hand side directional coupler. Hence, a_1 and a_2 are the field amplitudes of the light after propagating through the phase shifter and the drop port of the resonator, respectively, after being split off from the input field a_0 (see Eq. (1)). The splitting factor of the first directional coupler is given by the parameter t. The phase shifter imparts a phase shift, ϕ, while the transfer function of the micro-resonator, $A(\beta)$, modifies both the phase and amplitude of the signal. The two paths are then combined with a directional coupler, which is described by the classical beam splitter Eq. (2), where ε is the power splitting ratio, β is the wavevector, and a_i are shown in Fig. 1. The splitting ratio, ε, should be close to 50% for proper balanced operation.

$$a_1 = a_0 i \sqrt{t} e^{i\phi}$$
$$a_2 = a_0 \sqrt{1-t} A(\beta)$$

(1)

$$a_3 = \sqrt{1-\varepsilon}\, a_1 + i\sqrt{\varepsilon}\, a_2$$
$$a_4 = i\sqrt{\varepsilon}\, a_1 + \sqrt{1-\varepsilon}\, a_2 \tag{2}$$

The balanced detector, which generates the error signal, $Y(\beta)$, used for locking, differences the photocurrents of the two output ports of the MZI, and is described by Eq. (3), where α is the responsivity of the photodetectors, G is the transimpedance gain, $n/2Z_0$ is a constant representing the conversion from field amplitude to average optical power in the waveguide and a_m is the effective mode area. Expanding this relation gives the general formula for balanced homodyne detection for an arbitrary directional coupler ratio and phase shift. When used in a DWDM network, other wavelengths, which may simultaneously exist in the waveguide, beat with the filtered signal, a_2, at very high frequencies that are not resolved by the photodetector or the loop filter. Instead, a zero background error signal is maintained because the spurious signals are canceled by the balanced detector arrangement.

$$Y(\beta) = \alpha G \frac{a_m n}{2Z_0}\left[\,|a_3|^2 - |a_4|^2\,\right]$$
$$= \alpha G \frac{a_m n}{2Z_0} a_0^2 \begin{bmatrix} -2\sqrt{\varepsilon - \varepsilon^2}\,\sqrt{t - t^2}\left(A(\beta)e^{-i\phi} + A(\beta)^* e^{i\phi}\right) \\ + (2\varepsilon t - 2\varepsilon - t + 1)\,|A(\beta)|^2 + 2\varepsilon t - t \end{bmatrix} \tag{3}$$

In this paper, we investigate the locking of first-order filters and modulators only, so we consider the case of a simple ring resonator. The complex transfer function between through and drop port of a four port micro-resonator is given by Eq. (4), where κ is the resonator coupling coefficient (assumed to be identical for through and drop ports) and R is the radius of the ring or disk. Here, $\beta = 2\pi n_{eff}/\lambda$, where λ is the vacuum wavelength and n_{eff} is the effective index of the mode in the resonator.

$$A(\beta) = \frac{|\kappa|^4}{\kappa^2}\frac{e^{i2\pi R\beta}}{e^{i4\pi R\beta} + |\kappa|^2 - 1} \tag{4}$$

If we assume the directional coupler is perfectly balanced, and $\varepsilon = \frac{1}{2}$, then the BHL transfer function for the error signal reduces to Eq. (5) after substituting Eq. (4) into Eq. (3).

$$Y(\beta) = -\alpha G a_0^2\,|\kappa|^4\,\frac{a_m n}{Z_0}\sqrt{t - t^2}\left(\frac{e^{i\phi}}{\overline{\kappa^2}}\frac{e^{-i2\pi R\beta}}{e^{-i4\pi R\beta} + |\kappa|^2 - 1} + \frac{e^{-i\phi}}{\kappa^2}\frac{e^{i2\pi R\beta}}{e^{i4\pi R\beta} + |\kappa|^2 - 1}\right) \tag{5}$$

By plotting the BHL transfer function for various phase shifts, ϕ, between 0 and π, the shift in locking point with phase is apparent (Fig. 2). First, at zero phase shift, the error signal has an odd shape centered on resonance. By locking the loop to the zero crossing of the error signal, intensity noise fluctuations do not impart a shift in locking point. However, by varying the phase with a compact optical phase shifter, the zero crossing lock point can be shifted to the side of the resonance. In this way, an optical modulator can also be locked with the BHL technique. With a π phase shift, the slope of the error signal is inverted, which is useful for maintaining negative feedback in the control loop without adding an extra inverter circuit to the control electronics.

With a phase shift of $\pi/2$, the error signal no longer crosses through zero. Thus, to maintain a stable lock, the phase should be carefully controlled through proper design of the photonics. In general BHL is not employed for free space or fiber optic resonators since this requirement is only achievable in certain cavity geometries and is less robust than other methods [23]. However, high index contrast silicon photonics allows the entire MZI structure to fit within 20x30 μm^2, which renders common mode virtually all vibrations and thermal gradients.
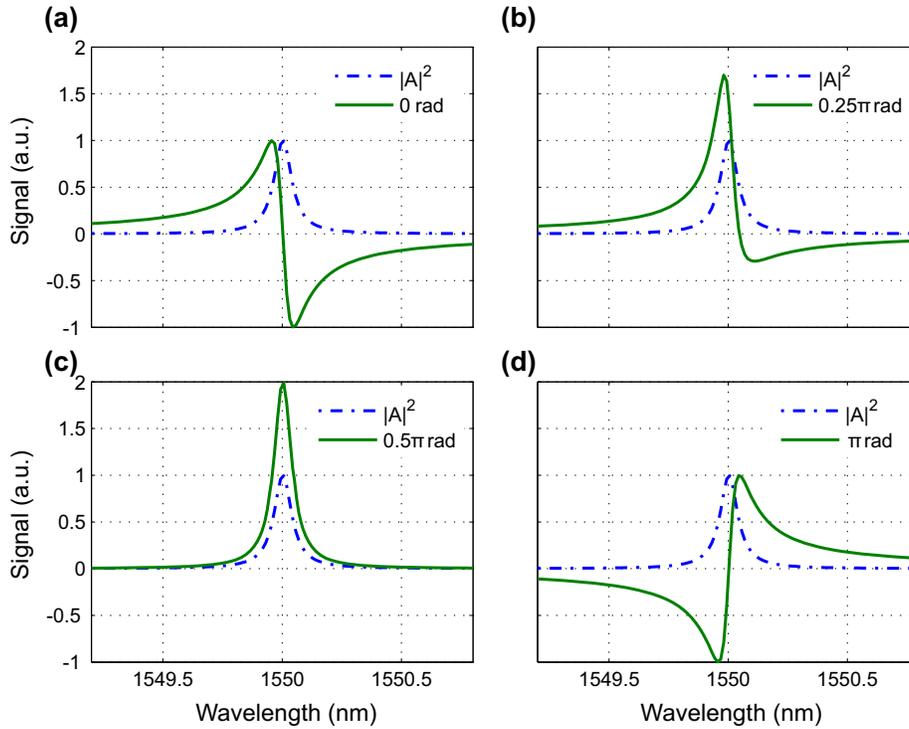
Fig. 2. The calculated transfer function for balanced homodyne locking (BHL) and the corresponding resonator drop port response are plotted above, for a critically coupled filter. (a)—(d) show the change in shape of the BHD transfer function for various relative phase shifts in the interferometer. (a) the ideal locking point for a filter is with no phase shift. (b) approximately ideal locking point for an on-off keyed modulator is at π/4. (c) no lock would be obtained for a π/2 phase shift. (d) the sign of the error signal can be inverted with a π phase shift.

3. Silicon photonic filter locking

To investigate the performance of balanced homodyne locking, we designed and fabricated an integrated photonic system with on-chip germanium photodetectors using our standard silicon photonics process [24]. The ring filter is based on the Adiabatic Resonant Micro-ring (ARM) described elsewhere [14], which is capable of broadband thermal tuning with the integrated heater. Our on-chip implementation, shown in Fig. 3, follows the same design given in Fig. 1, including a thermo-optic phase shifter, as described in [25]. The phase shifter has an electrical resistance of 6.25 kΩ, can sustain a maximum voltage of 16 Volts, and has an efficiency of 12.7 mW/π [25]. The present design makes no attempt to balance the path lengths or set the relative phase shift, which we adjusted post-fabrication with the phase shifter. In the present embodiment, the entire output of the filter's drop port is coupled into the interferometer. However, to lock a band-pass filter, the drop port power can be split or tapped before the interferometer.
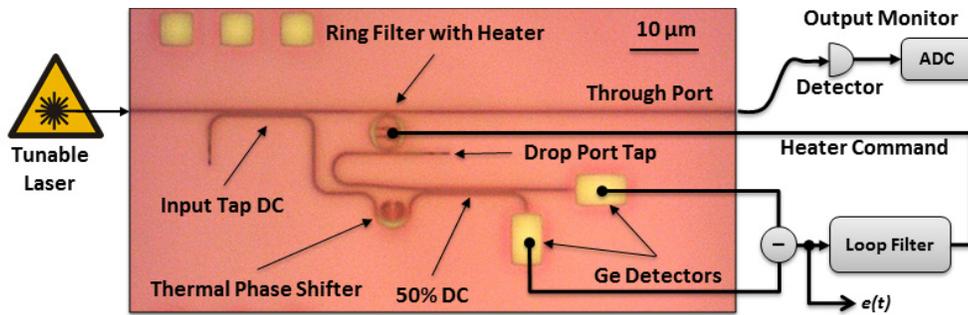
Fig. 3. An optical image of the filter locking system and corresponding experimental setup is shown above. A tunable laser provides the optical input to which the filter is locked. (ADC: analog to digital converter).

First, we measured the response of the error signal by sweeping a tunable laser through the filter resonance. An external transimpedance amplifier (Newfocus 2107) is connected to the integrated germanium photodetectors through an electrical micro-probe. The error signal, shown in Fig. 4, was measured for a range of voltages applied to the phase shifter. With no phase shift applied, the error signal is approximately symmetric, allowing the filter to be locked on resonance. However, by increasing the voltage, the shape is altered to allow for side locking, or even to fully invert the transfer function. Should post-fabrication adjustment be required to the locking point, a DC bias on the phase shifter can be set once.
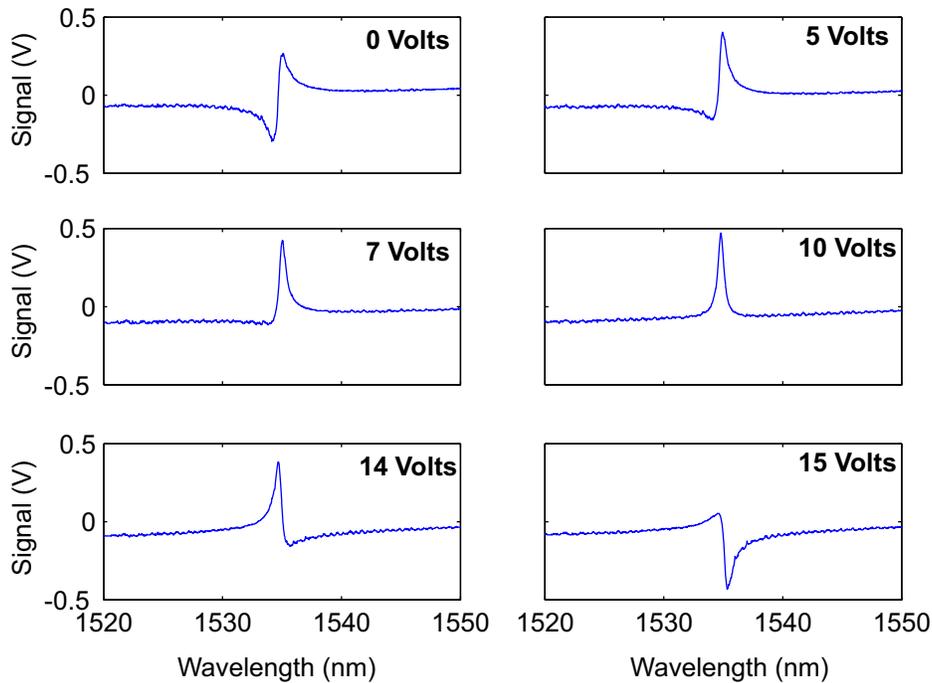

Fig. 4. The measured response of the balanced homodyne transfer function, using integrated germanium photodetectors, is shown above for various settings of the phase shifter voltage. At zero volts, the transfer function exhibits approximately zero relative phase imbalance, which is ideal for locking a filter. However, at 5 volts, the filter will be locked to the side of the resonance (suitable for our modulator), while at 10 volts there is approximately $\pi/2$ phase shift, and no lock would be obtained. At 14 and 15 volts, π phase shift is achieved, inverting the transfer function.

Finally, to test the locking performance, we continuously swept the tunable laser (Agilent 81640B) between 1532 and 1542 nm, recording the error signal, filter heater voltage and the through port power. For this test, we used a commercial PID controller (Stanford Research Systems SIM960) with only integral gain and a time constant of 100 kHz. However, we observe similar performance with a simple circuit consisting of a single op-amp integrator.

The test was recorded over 100 seconds, and is shown in Fig. 5, but could be extended indefinitely, limited by drift of the fiber probe station used for testing. The laser is swept at wavelengths just longer than the resonance of the filter so that the tuning mechanism, which can only heat the filter, can achieve an uninterrupted lock. Initially, the lock is disabled to show the variation in error signal and through port power as the filter goes near and away of resonance with the signal light. At 11 seconds, the integrator is enabled and the heater voltage is commanded to hold the error signal at zero. Consequently, the filter tracks the laser to hold the through port at minimum power, primarily limited by the extinction ratio of the filter, which is 6.1 dB. Some variation in through port power occurs as the laser is scanned, which is the result of power fluctuation in the tunable laser, the etalon formed by the waveguide end facets, wavelength dependent birefringence in the input fiber and polarization dependent loss in the waveguide, as well as slight variation in the shape of the balanced homodyne transfer function (see section 4). However, it is nevertheless apparent that the filter is held on resonance with the signal beam over the tuning range.
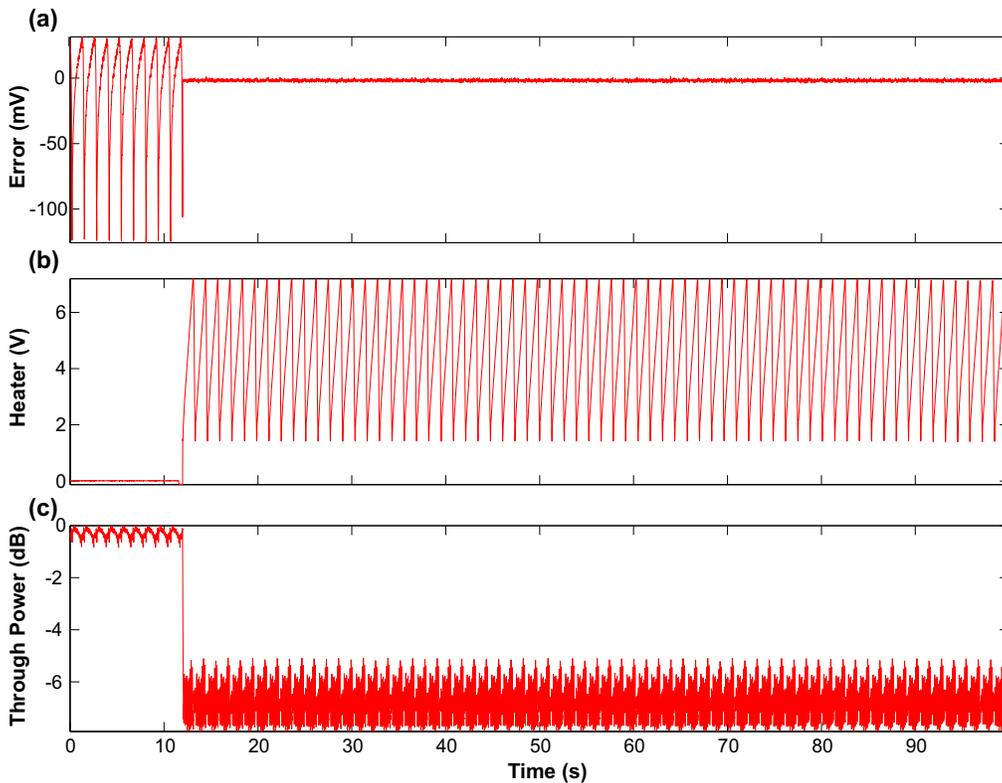

Fig. 5. Demonstration of the typical filter locking performance as the optical input wavelength is swept between 1532 and 1542 nm. Integrated germanium detectors were used for this test. The lock is enabled at 11 seconds, at which time the error signal **(a)** is driven to zero and the filter heater voltage **(b)** is driven so that the filter tracks the shifting wavelength. The relative optical power exiting the through port is shown in **(c)**.

4. Silicon photonic modulator locking

We also explored the application of balanced homodyne locking (BHL) to silicon photonic modulators as a potentially simpler method than bit error rate monitoring [18]. It is possible to use BHL for stabilizing a modulator because the modulation rate is significantly faster than the control loop bandwidth.

We adapted the photonic design shown in Fig. 3 to include a resonant disk modulator with an integrated heater, similar to the design in [2]. The modulator contains four terminals, two consisting of contacts to a vertical PN junction to modulate the carrier density in one half of the disk, while the other two contact a heavily n-type doped region near the center of the other side of the disk, to inject current for resistive heating. The modulator is driven with a 1.5 Volt peak-to-peak signal which is offset by −380 mV, spanning 370 mV to −1130 mV. In this way, the modulator is predominantly reversed biased in order to limit the accumulation of forward injected current to the vertical PN junction, as described in [26]. This modulator implementation, which serves to illustrate our locking method, is potentially RC limited by the geometry of the dopants. As a result, it achieved low error operation at 5-6 Gbit/s. An image of the fabricated device, without metal wiring, is shown in Fig. 6.
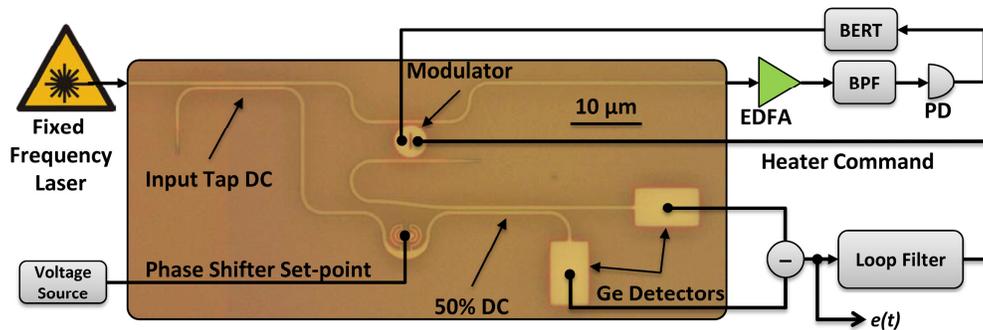

Fig. 6. An optical image of the balanced homodyne modulator locking device is shown above. The modulator is driven with a bit error rate tester (BERT) while locked. A phase shifter is adjusted to set the optimal locking point. The modulator loop filter is also a simple integrator, as used to lock the filter.

The modulation port of the resonator was driven with a commercial Bit Error Rate tester (Centellax TD1B1-A) at 5 Gbit/s with a pseudo-random bit stream (PRBS) of 2^{31}-1, 2^{23}-1 and 2^{15}-1 bit lengths. After modulation, the signal was coupled off chip, amplified in an erbium doped fiber amplifier (EDFA) pre-amp and filtered with a 1 nm bandwidth etalon (Newport TBF-1550-1.0). Finally, the signal was detected on a fiber coupled InGaAs photodetector and demodulated with the BERT. An eye diagram is shown in Fig. 7 for when the modulator is locked and driven with a PRBS signal at 5 Gbit/s, as measured on a sampling scope (Agilent 86100D with 83485A module).

To test the locking performance of the modulator, we varied the temperature of the entire silicon photonic chip with a thermo-electric cooler (TEC). In this way, we were also able to study the BHL performance under a uniform thermal variation.
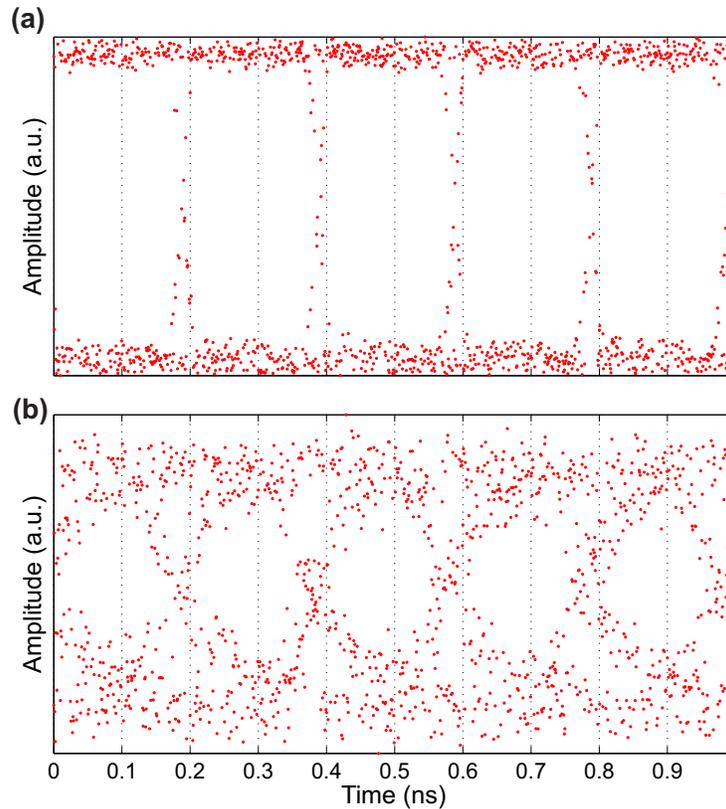
Fig. 7. An eye diagram is shown above for the modulator while locked to the laser line, with a pattern length of 2^{23}-1 bits and a data rate of 5 Gbit/s. **(a)** The driving electrical modulation signal from the pattern generator. **(b)** The received modulation signal after photodetection.

First, the modulator was locked to the signal light at 1545.8 nm by applying the loop filter output to the heater terminals, while the modulator was driven by the BERT. The wavelength of the signal light was adjusted so that at 60° C, the heater voltage was close to zero. Then, the voltage to the phase shifter was adjusted once to 6.6 volts, in order to minimize the bit error rate at 25° C. In this way, the laser line is locked to the side of the modulator resonance, as shown by the BHL transfer function in Fig. 9. The phase shifter voltage was not changed during the test. Then, the temperature was monitored with a thermistor while it was tuned between 5° and 60° C with the TEC. Temperature tuning below 5° C was not performed due to the buildup of frost and the limit of the TEC performance. Also, it was necessary to re-optimize the fiber-to-chip coupling at every temperature point due to thermal expansion in the aluminum waveguide mount.

Over a 55° C range, the BHD maintains lock, as shown in Fig. 8. We fully expect that the lock would be maintained at cooler temperatures. With a PRBS length of 2^{15}-1 bits, the link runs error free over an observation time of 120 seconds, except at 60° C, where it rises to $6 \cdot 10^{-12}$. With longer pattern lengths, the error rate is shifted higher, most likely due to the accumulation of carriers in the modulator during a long stream of identical bits. While there is some noise in the data because the fiber alignment must be manually maximized at each temperature to maintain coupling, the bit error rate is relatively flat over the full range, except at 60° C, where is begins to rise.
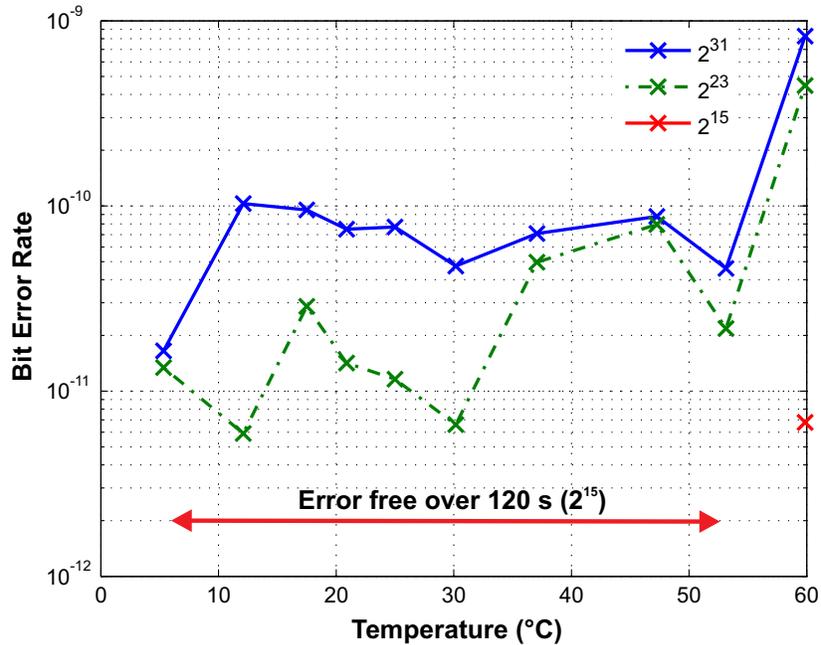
Fig. 8. The bit error rate of the modulator is measured at 5 Gbit/s for a fixed wavelength input as the temperature of the chip is varied from 5 °C to 60 °C The phase shifter voltage is left fixed at 6.6 volts. The measurement is performed with three different pattern lengths, owing to the characteristics of this particular modulator. With a pattern length of 2^{15} bits, no errors are observed until the temperature reached 60 °C. The coldest temperature measurable is limited by the performance of the thermo-electric cooler (TEC) and frost buildup on the chip. Integrated germanium photodetectors were used to lock the modulator wavelength to the signal wavelength.

The increase in bit error rate at high temperatures is likely due to slight variation in the phase of the interferometer as the modulator heater is tuned. To test this hypothesis, we measured the shape of the BHL error signal for the modulator at three different temperatures (5°, 30° and 60° C) while the heater voltage was varied to hold the resonant wavelength of the modulator fixed. This allows us to probe the shape of the error signal as it would exist while locked to a fixed wavelength. Figure 9 shows the measured error signal at the three temperatures, normalized in amplitude so that the relative shape is apparent. It can be seen that the lock moves more to the side of the resonance at higher temperatures. By comparison with Eq. (5), we estimate a 20° phase variation over this temperature range. As a result, we hypothesize that the heat applied to the filter induces a small phase shift in the interferometer waveguides.
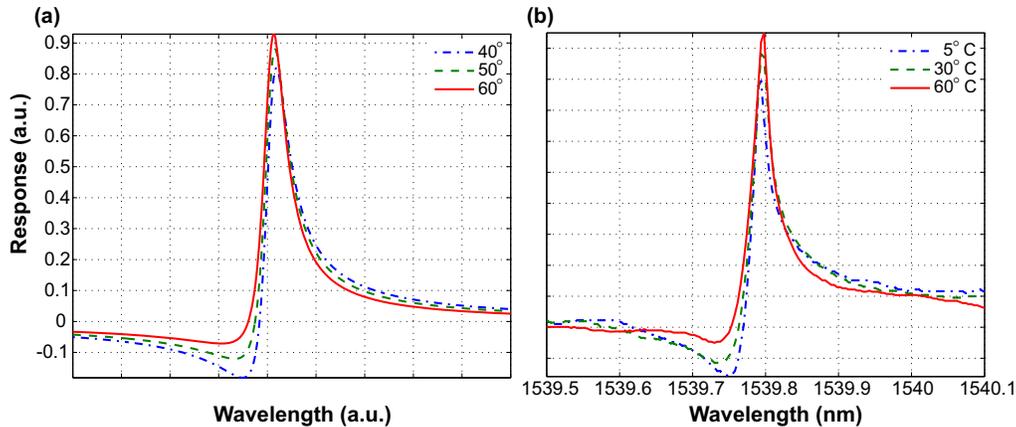
Fig. 9. The calculated **(a)** and measured **(b)** response for the balanced homodyne locking transfer function with the modulator is shown above. For **(a)**, the transfer function is shown for 40—60° phase shifts. For **(b)**, the transfer function for a modulator is measured for device temperatures of 5—60°C, with a corresponding heater voltage applied to hold the resonate wavelength constant. All transfer functions are normalized in order to compare the shapes. From comparison of **(a)** and **(b)**, it can be seen that the phase shift varies by about 20 degrees, which can explain the increase in bit error rate observed at 60°C—since the modulator would be locked too far from resonance.

5. Discussion and conclusion

We have demonstrated a technique for locking integrated micro-resonator filters and modulators based on balanced homodyne detection. The technique is insensitive to signal amplitude fluctuations and can be employed in a DWDM network. In addition, it requires the minimum amount of control circuitry, affording a compact implementation for practical on-chip photonic interconnects. Furthermore, since the micro-resonator is minimally disturbed, it is also a promising method for applications requiring very precise locking. With further work, we expect that the performance can be further enhanced. For instance, the design of the photonic system can be optimized to minimize thermal cross-talk between the heater and the interferometer, should an even wider thermal compensation range be required.

Acknowledgments